Osmotic spreading of *Bacillus subtilis* biofilms driven by an extracellular matrix

Agnese Seminara[a,b,1], Thomas E. Angelini[c], James N. Wilking[b], Hera Vlamakis[d], Senan Ebrahim[e], Roberto Kolter[d], David A. Weitz[b], and Michael P. Brenner[b]

[a]Genomes and Genetics Department, Unit Physics of Biological Systems, Institut Pasteur, F-75015 Paris, France; [b]School of Engineering and Applied Sciences, and Kavli Institute for BioNano Science and Technology, Harvard University, Cambridge, MA 02138; [c]Department of Mechanical and Aerospace Engineering, University of Florida, Gainesville, FL 32611; [d]Department of Microbiology and Immunobiology, Harvard Medical School, Boston, MA 02115; and [e]Department of Molecular and Cellular Biology, Harvard University, Cambridge, MA 02138

Edited by Raymond E. Goldstein, University of Cambridge, Cambridge, United Kingdom, and accepted by the Editorial Board November 6, 2011 (received for review June 23, 2011)

Bacterial biofilms are organized communities of cells living in association with surfaces. The hallmark of biofilm formation is the secretion of a polymeric matrix rich in sugars and proteins in the extracellular space. In *Bacillus subtilis*, secretion of the exopolysaccharide (EPS) component of the extracellular matrix is genetically coupled to the inhibition of flagella-mediated motility. The onset of this switch results in slow expansion of the biofilm on a substrate. Different strains have radically different capabilities in surface colonization: Flagella-null strains spread at the same rate as wild type, while both are dramatically faster than EPS mutants. Multiple functions have been attributed to the EPS, but none of these provides a physical mechanism for generating spreading. We propose that the secretion of EPS drives surface motility by generating osmotic pressure gradients in the extracellular space. A simple mathematical model based on the physics of polymer solutions shows quantitative agreement with experimental measurements of biofilm growth, thickening, and spreading. We discuss the implications of this osmotically driven type of surface motility for nutrient uptake that may elucidate the reduced fitness of the matrix-deficient mutant strains.

collective motility | gel swelling | surface translocation | bacterial biofilm | polymeric secretion

Bacterial biofilms are heterogeneous populations of differentiated bacteria that live in association with surfaces and exhibit a remarkable degree of spatio-temporal organization (1–3). The formation of a mature biofilm occurs in several stages, starting from the attachment of a single cell to a solid substrate. When cells commit to the surface, a protein- and sugar-rich polymeric extracellular matrix (ECM) is secreted in the extracellular space and holds the community together. Several different functions have been attributed to the ECM, ranging from protection to mechanical integrity and reserve of nutrient (4, 5). At the same time, flagella are downregulated, and most cells lose their individual motility. For the Gram-positive soil bacterium *Bacillus subtilis* the loss of flagella-mediated motility is genetically coupled to the production of extracellular matrix (6–10). This switch results in a slow kind of surface motility that allows the biofilm to spread outward on the substrate. Although spreading has been attributed to a qualitative concept of "pushing" associated with biomass growth, the physical force generating mechanism that drives biofilm expansion outward across a surface is not known. One intriguing possibility is the potential contribution of the ECM to biofilm growth; the ECM is a highly visco-elastic and sticky substance, and it might be expected to hinder expansion rather than facilitate it (4, 5). However, the ECM clearly plays a crucial role in biofilm, and its possible effect in the actual expansion of the biofilms has never been investigated.

Here, we demonstrate that, in the first 24 h of biofilm development, extracellular matrix production drives *B. subtilis* biofilm spreading and that, by contrast, flagellar motility does not contribute appreciably to biofilm spreading. Moreover, mutants lacking the exopolysaccharide (EPS) component of the ECM show a dramatically reduced surface motility, even if their division rate in shaking culture is similar to that of the wild type. We propose that spreading is primarily driven by osmotic stresses generated collectively by secretion of EPS in the extracellular space. We develop a theoretical model of the resulting motion that quantitatively predicts the evolution of the shape of a wild-type biofilm. Without the EPS, the biofilm cannot generate osmotic pressure, leading to reduced spreading. Thus, the limited spreading of a mutant defective in EPS production may be attributed to an alternative and less effective force generating mechanism: Cells at the leading edge are arranged in a tightly packed monolayer, and at each cell division they interact directly with their neighbors and push the monolayer forward. This cell–cell interaction has been previously argued to drive bulk spreading in bacterial colonies (11). Although the shape of the wild-type biofilm is inconsistent with this notion, we find that this could apply to the mutant. Moreover, the lack of EPS-driven spreading limits nutrient uptake, which may elucidate the reduced fitness of the mutant (12).

Results and Discussion

Biofilm Spreading. Spreading of *B. subtilis* biofilms on agar plates depends on extracellular matrix production. We inoculate an initial 0.5-μL drop of cells at OD_{600} of 1 on an agar plate containing the biofilm promoting medium MSgg (see *Materials and Methods*) and store it in a saturated humid incubator at 30 °C. As the cells grow and divide, the colony thickens and matrix production marks the onset of differentiation and biofilm formation (10). The base of the biofilm then expands, with an approximately fivefold increase in radius over 24 h (Fig. 1*A*, *Top*, and *B*). We compared colony expansion of wild-type cells and a mutant lacking flagella (*hag*), which are required for swimming and swarming motility in *B. subtilis*. The *hag* mutant colony displayed a very slight reduction in colony size that was not statistically distinct from the wild type (Fig. 1*A*, *Middle*, and *B*). In contrast, we observed that the production of EPS was crucial for biofilm spreading. Without the genes responsible for the exopolysaccharide component of the matrix (*epsA-O*, hereafter referred to as *eps*), there was a dramatic decrease in horizontal expansion Fig. 1*A*, *Bottom*, and *B*. These observations agree well with recent data (12) demonstrating that the wild-type biofilm eventually produces more cells than the *eps* (see *Discussion*). The dramatically differ-

Author contributions: A.S., T.E.A., R.K., D.A.W., and M.P.B. designed research; A.S., T.E.A., J.N.W., H.V., and S.E. performed experiments; A.S. and M.P.B. performed theoretical analysis; and A.S., T.E.A., J.N.W., H.V., R.K., D.A.W., and M.P.B. wrote the paper.

The authors declare no conflict of interest.

This article is a PNAS Direct Submission. R.E.G. is a guest editor invited by the Editorial Board.

[1]To whom correspondence should be addressed. E-mail: seminara@seas.harvard.edu.

This article contains supporting information online at www.pnas.org/lookup/suppl/doi:10.1073/pnas.1109261108/-/DCSupplemental.

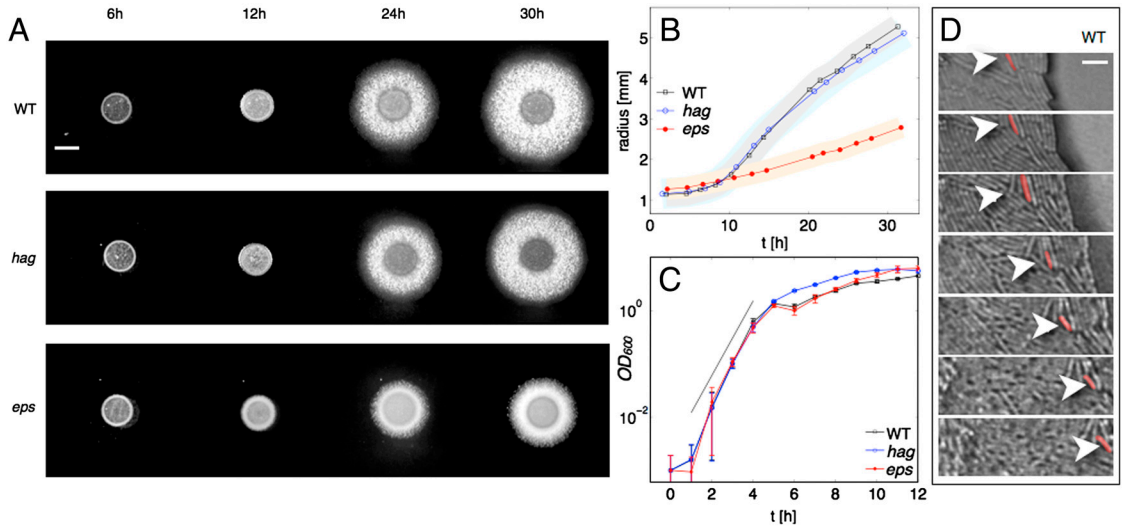

Fig. 1. Biofilm expansion is a collective mechanism based on extracellular matrix production. (*A*) Top view of *B. subtilis* biofilm morphology and expansion on MSgg agar plates at different timepoints for wild-type (WT) strain 3610 (top row), the flagella mutant *hag* (mid row), and the *eps* mutant (bottom row). Scale bar, 1 mm. A central spot is apparent in all the pictures and represents the initial inoculum of cells. (*B*) Radial growth obtained by averaging every two hours over 25 colonies for each of the three strains WT (black squares), *hag* (blue open circles), and *eps* (red dots); shades indicate the standard deviation. The *eps* mutant shows a severely limited horizontal expansion. In these conditions, flagella do not play a significant role in the horizontal expansion of the biofilm. (*C*) Growth curves of the three strains: WT, *hag* and *eps* in shaking liquid culture. (*D*) Consecutive frames from a time-lapse high resolution movie of the edge of the growing wild-type biofilm. The marker indicates the position of a particular cell that slides on top of the agar during expansion.

ent expansion of the *eps* mutant is not due to a general growth defect. In fact, the wild type, *hag*, and *eps* strains follow similar growth curves in shaking cultures at 37 °C, where cells do not appreciably produce extracellular matrix (see Fig. 1*C*). This led to the hypothesis that the production of EPS itself could function to enhance colony spreading.

Physical Mechanism and Mathematical Model. How can extracellular matrix secretion enhance spreading? Based on the experiments, we hypothesize that the EPS concentration causes an increase in the osmotic pressure, causing swelling of the biofilm, through uptake of water from the agar. Swelling of gels is common (13), and the propensity for swelling depends on the physical properties of the gels. In principle, osmotic gradients could also occur from sources other than the EPS itself—i.e., gradients of small molecules (nutrients, ions, etc)—though such gradients would be similar in wild type and *eps*, and hence are inconsistent with our observations.

To test this hypothesis, we develop a mathematical model to predict how the shape of a biofilm would change in response to osmotic pressure gradients due to EPS secretion. By quantitatively comparing these predictions to the experiments, we test and prove this proposed mechanism. The model considers the biofilm as a mixture of biomass and water with a biomass volume fraction ϕ and water volume fraction $1-\phi$. The biomass volume fraction is the sum of cells and matrix volume fraction ϕ_c, ϕ_m. We can write an equation for the total volume fraction $\phi=\phi_c+\phi_m$ under the assumption* that $\phi_m \ll \phi_c$ (see *Materials and Methods* and *SI Text*). Water can flow from the agar substrate to the biofilm through osmotic pressure gradients. When the biofilm is in equilibrium with the agar, the biofilm volume fraction is a constant ϕ_∞, so that the osmotic pressure in the biofilm equals that in the agar. Spreading forces are generated in the biofilm as cells consume water and nutrient to produce biomass, creating an osmotic imbalance in the colony. Biomass growth modifies ϕ from its equilibrium value according to mass conservation for water and biomass:

$$\partial_t\phi+\nabla\cdot(\phi\mathbf{v}_b)=g\phi \qquad [1]$$

$$\partial_t(1-\phi)+\nabla\cdot[(1-\phi)\mathbf{v}_w]=-g\phi \qquad [2]$$

where g is the rate of production of biomass and $\mathbf{v}_b$, $\mathbf{v}_w$ are the average velocities of the biomass network and of water. The increase in biomass volume fraction draws water from the agar substrate to equilibrate the osmotic imbalance. To describe the dynamics generated by this deviation from osmotic equilibrium, we minimize the sum of mixing free energy change and dissipation (14) and obtain equations for the space-time distribution of $\mathbf{v}_b$, $\mathbf{v}_w$:

$$\mu_b\nabla^2\mathbf{v}_b=\nabla(p+\pi) \qquad [3]$$

$$\zeta(\mathbf{v}_w-\mathbf{v}_b)+(1-\phi)\nabla p=0 \qquad [4]$$

where we model the biomass network as a viscous fluid with viscosity μ_b; $\zeta\sim\mu_w/\xi^2$ is the water-network friction coefficient (15, 16) and ξ is the mesh size of the network. Water flow is highly obstructed by the presence of the network, so that Eq. **4** is essentially Darcy's law for water speed relative to the network (see *Materials and Methods*). Eqs. **1**–**4** with a constitutive equation for $\pi=\pi(\phi)$ and $\xi=\xi(\phi)$ and boundary conditions constitute our model (see *Materials and Methods* and *SI Text*).

To analyze the mathematical model, we consider small departures from osmotic balance, expanding $\phi=\phi_\infty+\delta\phi$ and $\xi=\xi_\infty+\delta\xi$. We also note that the height of the biofilm is always about 10 times smaller than its radius R, which reduces the model equations to a single partial differential Eq. **5** for the height $h(r,t)$ of the biofilm as a function of radial distance r; this is the so-called lubrication approximation (see *SI Text* and, e.g., ref. 17):

$$h_t-\frac{1}{3(1-\phi_\infty)^2}\frac{\mu_w}{\mu_b}\frac{R}{\xi_\infty^2}\frac{1}{r}[rh^3(gh)_r]_r=gh \qquad [5]$$

This equation represents that the change in shape of the biofilm is due to the competition between vertical growth (the right hand side) and horizontal spreading (the second term on the left).

*This can be easily verified by imaging a cross-section of the biofilm or by purifying the extracellular matrix as described in (27).

Let us assume that the colony has an initial height h_0 and radius R_0; if h_0 is small then initially the vertical swelling is much larger than horizontal spreading. This is captured by the dimensionless parameter representing the ratio of the swelling to horizontal spreading.

$$K = \frac{1}{3(1-\phi_\infty)^2}\frac{\mu_w}{\mu_b}\frac{h_0^3}{\xi_\infty^2 R_0}. \quad [6]$$

However, because h grows exponentially and $R \sim$ constant, we expect K to increase and eventually the horizontal flux takes over, marking the transition between vertical swelling and horizontal spreading.

This transition is observed in numerical simulations of the model, Fig. 2*A*. We carry out the simulations by starting with an initial inoculum of bacteria, which spreads on a very thin layer of thickness h_∞; this gets rid of a putative singularity in the slope of the solution at the edge of the colony and emulates the experiments where the colony spreads on a very thin layer of cells. This prewetting layer is also a simple way to avoid detailed modeling of the contact line whose dynamics is beyond the scope of this paper. We define the radius of the colony as the point where the slope h_r^* is maximally steep, marking the edge of the bulk of the biofilm (see Fig. 2*A*). The radius so defined is a good candidate for the comparison with the experimental profiles presented in Fig. 3 because it does not depend directly on the unmodeled dynamics of the contact line. Fig. 2*B* then shows the radius as a function of time for different values of K. The simulations show that initially the radius of the colony does not spread; but there is a time, depending on K, at which the colony starts spreading horizontally.

We can quantitatively capture this transition by looking for a self-similar solution of Eq. **5** of the form $h = \frac{1}{R^2}F(\frac{r}{R})e^{gt}$. Using this ansatz in the equations of motion, we obtain (see *Materials and Methods*) the solution

$$\frac{h}{h_0} = \frac{e^{gt}}{(R/R_0)^2}\left(1 - \frac{3}{2}\frac{r^2}{R^2}\right)^{1/3} \quad [7]$$

$$\frac{R}{R_0} = \left[1 + \frac{7}{3}K(e^{3gt}-1)\right]^{1/7}. \quad [8]$$

The similarity solution predicts that the radius $R(t)$ is initially constant but then starts to grow exponentially when $7/3Ke^{3gt} \sim 1$; beyond this time, the radius grows exponentially according to the law $R \sim R_0 e^{\frac{3}{7}gt}$. To characterize the transition we compute the slope h_r^* at the edge of the biofilm defined as the point where the magnitude of the slope is the largest; According to the similarity solution Eq. **7**, this is given by

$$h_r^* \sim \frac{h_0}{R_0}\sqrt{\frac{2}{3}}\frac{e^{3gt}}{(h_\infty/h_0)^2(R/R_0)^7}. \quad [9]$$

The experimental data presented in the next paragraph suggest that in fact the thin layer of cells ahead of the bulk of the biofilm grows vertically. To mimic this property we let $h_\infty = h_\infty^0 e^{gt}$. Eqs. **8** and **9** then predict that initially the biofilm steepens ($h_r^* \sim e^{gt}$) without spreading ($R \sim R_0$); at the critical time when $Ke^{3gt} \sim 1$, the biofilm undergoes expansion and smoothening as $h_r^* \sim e^{-2gt}$. The transition is completely determined by the single nondimensional parameter K: The biofilm starts to expand at a critical time $\sim \log(K^{-1/3})$ when the profile has reached a critical slope $\sim K^{-1/3}$. Fig. 2 *A–D* shows the transition as obtained by numerical simulations of Eq. 5 in a flat geometry for different values of K. For small values of K the biofilm transitions to expansion at a later time and at a steeper critical slope. Control over this parameter would be an effective method for biofilms to purposely modify their expansion.

Comparison with Experiments. Time-lapse microscopy shows that wild-type biofilms first swell vertically and then undergo spreading, as predicted theoretically. To show these two stages of growth, we measured the full three-dimensional shape of the biofilm at regular intervals of 45 min for the first 18 h of biofilm growth. First we recorded simultaneously the transmitted light from a growing biofilm and a side view picture; we then verified that the maximum transmitted light correlated well with the maximum thickness of the biofilm (see *SI Text* and Fig. S1) and assumed that the same calibration holds everywhere in the biofilm. We collected the 2D transmitted intensity maps for both wild-type and *eps* growing biofilms (see *Materials and Methods*), and we averaged azimuthally to obtain the profiles shown in Fig. 3 *A–B*. Initially, the wild-type biofilm swelled vertically (first four curves in Fig. 3*A*) and it then transitioned to horizontal spreading (last six curves in Fig. 3*A*).

The wild-type shape transition quantitatively matched our theory of osmotic swelling. To visualize the transition and compare the experimental data with the theory we traced the maximum slope on the profiles in Fig. 3*A*: During the initial swelling the profiles steepened and the radius remained constant; at the onset of spreading, the radius started to expand and the biofilm smoothed out. In Fig. 3 *D* and *E* we show the slope and the radius of the biofilm as a function of time, rescaled with the average doubling time $g^{-1} \approx 2.3$ h inferred from volume growth (see Fig. 3*C*). A comparison of the maximum slope to the theoretical prediction **9** provides the value of the sole fitting parameter $K \approx 10^{-5}$. With g and K so determined, Eq. **8** completely deter-

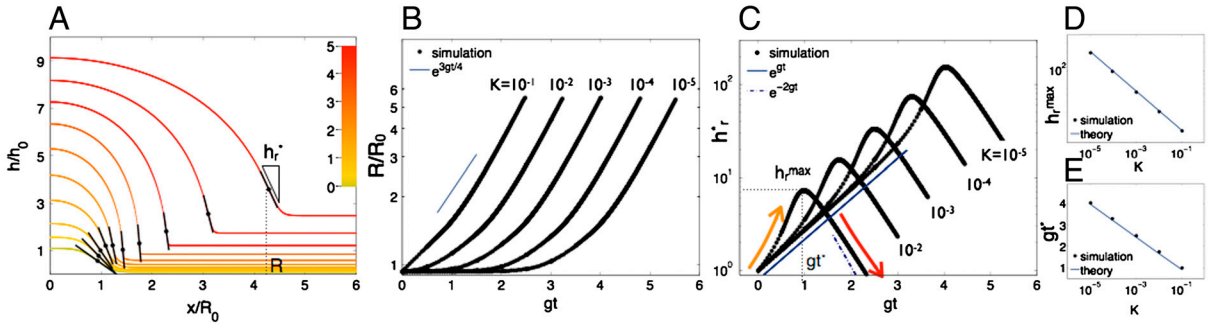

Fig. 2. A model of osmotically driven growth predicts a transition between an initial vertical swelling and a later horizontal expansion, as illustrated by simulations and asymptotics of the model equations. The single nondimensional parameter K controls the transition. (*A*) Simulated profiles for $K = 10^{-5}$ at different times color coded from green at $tg = 0$ to red at $tg = 5$. The edge of the biofilm is marked on each profile through the slope h_r^*. (*B*) Radius of the biofilm defined as the point where the profile is maximally steep; the black circles represent the results of simulations of Eq. **5** in two planar dimensions, for different values of K from 10^{-1} to 10^{-5}; the blue lines are the asymptotic scalings given by the self-similar solution **7**–**9** modified for planar coordinates (see *Materials and Methods*). (*C*) The slope at the edge of the colony initially increases as the biofilm swells vertically as indicated by the arrow. After reaching the critical value h_r^{max}, it decreases as the biofilm expands and smoothens; the maximum (critical) slope defines the transition time (symbols as in *B*). (*D*) Critical slope and (*E*) time of transition as a function of K (symbols as in *B*).

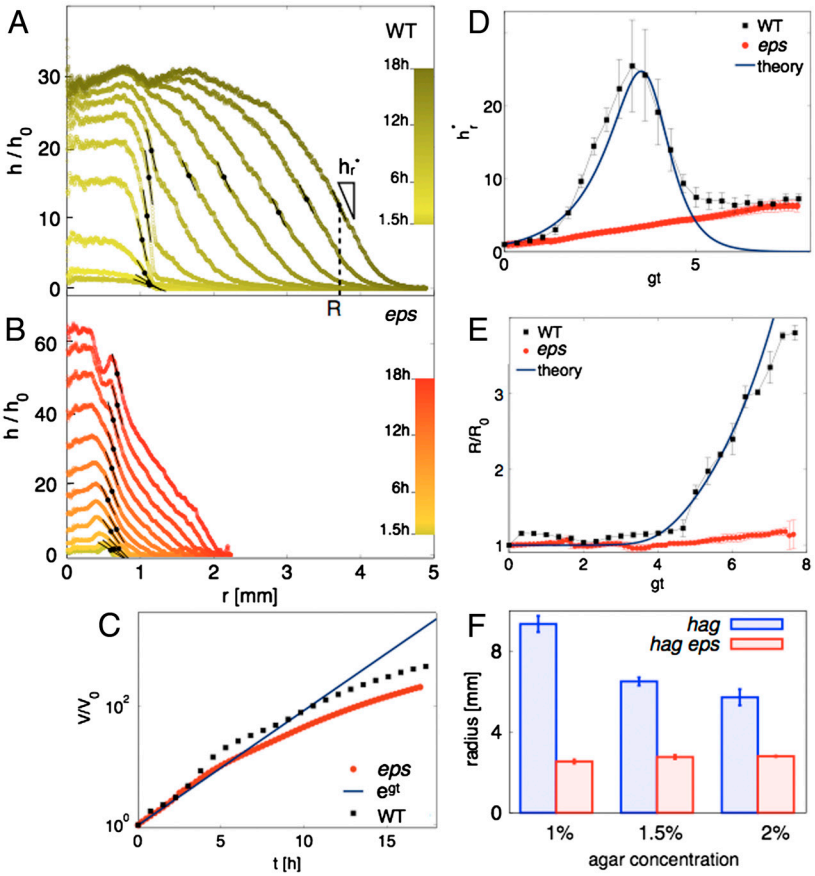

Fig. 3. Quantitative comparison with experimental data of biofilm profiles shows that the wild type undergoes the predicted swelling/spreading transition, whereas the *eps* mutant does not. Biofilm shape at intervals of 1.5 h for WT (*A*) and *eps* mutant (*B*), obtained by azimuthally averaging the logarithm of the transmitted light intensity (see *Materials and Methods* and *SI Text*). The profiles are shown in units of the initial height h_0 defined as the average height in the central plateau of the biofilm at time 0; we show the time evolution color-coded from green at $t =$ 1.5 h to dark green (WT) and red (*eps*) at $t = 18$ h. (*C*) Volume of the biofilm as a function of time, calculated from the profiles in *A* and *B*. We obtain the average doubling time by fitting the wild-type growth curve with a single exponential giving $g^{-1} \sim 2.3$ h. (*D*) The maximum slope of the wild-type biofilm (black squares) first increases when the biofilm swells vertically and then decreases as the biofilm spreads horizontally and smoothens out. Values are shown in units of the initial value. Time is nondimensionalized with $g^{-1} = 2.3$ h obtained from the previous fit. The experimental points closely follow the theoretical prediction **9** with the single fitting parameters $K \sim (1 \pm 0.2) \times 10^{-5}$. The *eps* mutant (red circles) continues to steepen, with no apparent shape transition. (*E*) Wild-type biofilm radius (black squares) starts to expand after a critical time; *eps* biofilms (red circles) do not display the transition. Data for the wild type are in good agreement with the prediction **8**. The radius is defined as the point of maximum slope and it is computed from the profiles. Error bars in *D* and *E* are defined as described in *Materials and Methods*. (*F*) Average horizontal extension of *hag* (blue) and *hag eps* (red) biofilms after 30 h from plating as a function of agar concentration. The error bar is the standard deviation computed over three replicas. Data are obtained with the protocol described in *Radial growth*.

mines the evolution of R with no free parameters: The experimental data accord well with the theory as shown in Fig. 3*E*.

The only significant discrepancy between the theory and the experiments is the long time behavior of the slope h_r^*: Fig. 3*D* shows that the experiments asymptote to a constant slope, whereas the theory predicts that the slope asymptotically vanishes. The reason for this discrepancy can be traced to the fact that in the experiments the growing monolayer of cells extends for a finite length out of the colony. When the biofilm starts spreading, the bulk may reach the contact line, depending on how fast they move relative to each other. To capture this effect and predict the finite asymptote of the slope in Fig. 3*D*, one should model the precise physical mechanisms governing the leading edge (including the wetting properties of agar, nutrient depletion, surfactant effects), which are beyond the scope of the current work. Note that typically contact line problems are sensitive to microscopic variations in the properties of the surface, and therefore we expect the asymptote to be highly variable from one replicate to another.

The parameter K is a combination of geometric and material parameters (see Eq. **6**). While the geometric parameters can be easily obtained—for our experiments $h_0 \approx 1$ μm and $R_0 \approx$ 1 mm—the material parameters are more difficult to measure in vivo, without disrupting biofilm integrity. Estimates of biofilm viscosity vary widely for different biofilms (see, e.g., refs. 18 and 19), which is not surprising considering that biofilms grow in disparate conditions. We measured biofilm viscosity through creep tests by collecting 25 biofilms grown on agar plates for 20 h (see *SI Text*), and we obtained $\mu_b \approx 100$ Pa · s. These values for R_0, h_0, μ_b, together with our fit for K, provide an estimate for the mesh size $\xi_\infty = 20$ to 70 nm (for $\phi_\infty = 0.2$ to 0.8) which is in the range of values recently published in ref. 20. We thus conclude that the agreement of the data with the theory of osmotic motility occurs at a sensible value of K, consistent with previous measurements.

The *eps* mutant biofilm cannot effectively generate osmotic pressure because without the exopolysaccharide component of the matrix, the biofilm reduces to a suspension of cells with a concentration of extracellular polymers dramatically reduced. The osmotic pressure of a particle suspension is inversely proportional to the volume of the particles and vanishes when these are larger than approximately 1 μm (see, e.g., ref. 21). The mutant is then unable to generate osmotic forces and we expect its growth history to be entirely different from that pictured by our osmotic theory. Consistent with this argument, none of the theoretical predictions applies to the mutant: The profiles shown in Fig. 3*B* do not display any shape transition; the radius remains constant throughout the first 20 h (see Fig. 3*E*, red circles) and the slope always increases never changing the trend (see Fig. 3*D*, red circles). To further prove the profound difference between the expansion with and without polymers, we varied the agar concentration from 1% to 2% and compared the rate of expansion for *hag* biofilms and *hag eps* double mutants. In this manner we would solely be looking at the effect of agar concentration on EPS-mediated spreading, independent of any flagella-mediated surface motility. The theory predicts that, in the presence of polymers, the external osmotic pressure determines the value of K and thus affect the rate of expansion. The results confirm this trend (see Fig. 3*F* and Fig. S2): While the *hag* mutant colony radius decreased with increasing agar concentrations, the *hag eps* mutant colony radius remained the same.

Discussion. Although the shape of the *eps* mutant never changes, the very edge of the biofilm does spread slowly over time. In the absence of osmotic forces, the matrix-deficient mutant may spread owing to an alternative mechanism based on cell–cell contact and called "sliding" (see e.g., refs. 11 and 22–25): At the external edge of the biofilm the cells are tightly packed so that they directly push their neighbors at each cell division. To show

this arrangement, we monitored the leading edge of the biofilm and followed cell position individually: Fig. 1*D* shows that the cells slide over the agar and are organized in a tightly packed monolayer as previously observed for other bacterial colonies (11).

We may then distinguish two profoundly different mechanisms for flagella-independent surface motility: Osmotic gradients push wild-type expansion from the bulk, whereas cell–cell contact drives expansion of the matrix-deficient mutant from the leading edge. The wild-type biofilm undergoes a shape transition determined by a combination of geometric and material parameters potentially under genetic control. Control over the shape transition is an invaluable opportunity for the wild-type biofilm to increase nutrient uptake. In fact, any microcolony feeding on diffusing nutrients hits a severe growth bottleneck due to nutrient depletion if it is not able to change shape. This is because nutrient uptake by diffusion is approximately proportional to the surface area of the colony, whereas consumption is proportional to the volume. If the colony grows without changing shape, its volume grows faster than its surface and eventually uptake cannot keep up with consumption. When consumption equals uptake, starvation occurs: An increasing portion of the colony is starved and the fraction of cells that continue to grow is limited to an ever thinning external shell of the colony. Any microcolony feeding on diffusing nutrients faces this very general problem and many species have evolved different ways to cope with growth bottlenecks (see e.g., ref. 26). The wild-type biofilm is able to break this bottleneck by changing shape and increasing the fraction of growing cells thus speeding up growth. This result may in fact elucidate the reduced fitness of the *eps* mutant that—despite a growth curve that is similar to the wild type in shaking culture—displays a reduced growth rate under biofilm conditions (12). This result strongly suggests that the energetic investment implied in the production of EPS is rewarded by the consequent increase in nutrient uptake and results in a net fitness increase for the colony.

Not all biofilms are able to spread under osmotic forces. In the presence of EPS, our theory predicts osmotic spreading for biofilms that behave like viscous fluids. However, biofilms are complex heterogeneous materials and their behavior may resemble that of a fluid or that of a solid depending on many factors including composition and external conditions (20). The *sinR* mutant, lacking the master regulator of matrix gene expression SinR, is an example of solid-like behavior. Structural integrity of *B. subtilis* biofilms is provided by the interaction between EPS and TasA, a major protein component of the extracellular matrix (6, 27, 28). As a result, *sinR* mutants, that greatly overproduce both EPS and TasA, are very hard, hyperwrinkled colonies and are extremely difficult to tear apart (7). Clearly, *sinR* biofilms on MSgg plates can no longer flow and the increased EPS concentration in these biofilms induces stretching of the biomass network, rather than outward flow and spreading. Consistent with this notion, *sinR* biofilms appear smaller than the wild type.

Materials and Methods

Bacterial Culture. *B. subtilis* biofilms are grown according to protocols adapted from ref. 29. *B. subtilis* cells (strain 3610) are streaked from −80 °C freezer stocks onto 1.5% agar LB medium plates and incubated at 37 °C for 12 hours.

Growth curves. After incubation cells are resuspended in LB and diluted to OD_{600} of 0.001, incubated on a shaker at 37 °C and the OD is measured every hour.

Radial growth. After incubation, cells are resuspended in LB and diluted to OD_{600} of 1. A drop of 0.5 μL is spotted onto a 1.5% agar plate containing minimal salts glycerol glutamate (MSgg) medium (29) with 0.25% glycerol and 0.25% glutamate. For the experiment presented in Fig. 3*F* and *SI Section II* we plated 1 μL on 1%, 1.5% and 2% agar plates. Strains used in this study: wild-type (NCIB3610), *eps* (3610 epsA-O::tet), *hag* (3610 hag::tet) and *hag eps* (3610 epsA-O::tet, hag::mls). After the droplet of bacteria dries, the sample is transferred to a humidified chamber on a dissecting scope and kept at 30 °C. For every time point, images are analyzed by tracing the edge of the colonies and calculating the area A for each biofilm at each time point. The radius for Figs. 1*B* and 3*F* and Fig. S2 is defined as $\sqrt{A/\pi}$.

Time-lapse microscopy. After incubation (*Bacterial culture*), 3 mL of LB liquid medium is inoculated with cells from an isolated colony. The inoculated LB medium is incubated on a shaker at 37 °C for 3 h, when the optical density of the bacteria solution is 0.6. Approximately 0.5 μL of the bacteria solution is spotted onto a 1.5% agar plate containing minimal salts glycerol glutamate (MSgg) medium (29) with 0.25% glycerol and 0.25% glutamate. After the droplet of bacteria dries, the sample is transferred to a humidified chamber on an inverted microscope and kept at 30 °C. Each 45 min, automated data collection and stage control software collects a 9×9 grid of transmission-mode bright-field images; images are stitched together and processed with custom written MATLAB software. Bright-field images are converted to thickness maps by employing the Beer–Lambert law, $I(\mathbf{r}) = I_0 e^{-h(\mathbf{r})/\lambda}$ where I_0 is the average light intensity incident on the biofilm, and λ is an absorption length that is measured as described in the *SI Text* (see Fig. S1). The 2D thickness map, $h(\mathbf{r})$, is integrated over the azimuthal angle to produce the 1D thickness profile, $h(r)$.

Mathematical Model. The biofilm is a heterogeneous material mainly composed of water, cells and extracellular matrix. To model the biomass we extend classic Monod models by adding the production of an extracellular matrix, and we obtain two continuity equations for the cells volume fraction ϕ_c and the matrix volume fraction ϕ_m (see *SI Text*). It appears from imaging the biofilm at high magnification that cells are highly packed so that we assume $\phi_m \ll \phi_c$ and we write a single equation of continuity for the biomass volume fraction $\phi = \phi_c + \phi_m$ (Eq. **1**). Under this assumption, the biofilm reduces to a two-phase material where the two phases are extracellular water and biomass. Mass conservation for water results in Eq. **2**. The sum of Eqs. **1** and **2** yields:

$$\nabla \cdot \mathbf{v} = 0 \qquad \textbf{[10]}$$

where $\mathbf{v} = \phi \mathbf{v}_b + (1-\phi)\mathbf{v}_w$ is the volume averaged velocity.

In the absence of biomass production, the biofilm reaches mechanical and thermodynamic equilibrium with the environment (agar). We are interested in the description of small departures from equilibrium caused by a slow biomass production. In quasi-static conditions, the equations of motion in the presence of dissipations can be obtained by minimizing the sum of free energy change and dissipation (14): $R = \int d^3r \zeta |\mathbf{v}_b - \mathbf{v}_w|^2/2 + \underline{\underline{\sigma}}_w \cdot \nabla \mathbf{v}_w + \underline{\underline{\sigma}}_b \cdot \nabla \mathbf{v}_b - \partial f/\partial\phi \nabla \cdot (\phi \mathbf{v}_b - g\phi) - p\{\nabla \cdot [\phi \mathbf{v}_b + (1-\phi)\mathbf{v}_w]\}$ with respect to $\mathbf{v}_b$ and $\mathbf{v}_w$. Here $\zeta \sim \mu_w/\xi^2$ is the water-network friction coefficient (15, 16); $\underline{\underline{\sigma}}_w$, $\underline{\underline{\sigma}}_b$ are the stress tensors of water and biomass network; $f(\phi)$ is the mixing free energy and p (pressure) is the Lagrange multiplier enforcing total volume conservation **10**. The equations of motion then read:

$$\zeta(\mathbf{v}_b - \mathbf{v}_w) - \nabla \cdot \underline{\underline{\sigma}}_b + \phi \nabla \frac{\partial f}{\partial \phi} + \phi \nabla p = 0$$

$$\zeta(\mathbf{v}_w - \mathbf{v}_b) - \nabla \cdot \underline{\underline{\sigma}}_w + (1-\phi)\nabla p = 0$$

where we can rewrite $\phi \nabla \frac{\partial f}{\partial \phi} = \nabla \pi$ by definition of osmotic pressure $\pi = \phi \partial f/\partial\phi - f$. We consider both phases to be Newtonian fluids with viscosities μ_w and $\mu_b \gg \mu_w$. By neglecting water–water friction,† which is typically much smaller than network–water friction in many synthetic gels (see refs. 16 and 31) we obtain:

$$\zeta(\mathbf{v}_b - \mathbf{v}_w) - \mu_b \nabla^2 \mathbf{v}_b + \nabla \pi + \phi \nabla p = 0 \qquad \textbf{[11]}$$

$$\zeta(\mathbf{v}_w - \mathbf{v}_b) + (1-\phi)\nabla p = 0 \qquad \textbf{[12]}$$

Eq. **12** is essentially a Darcy's law for the relative motion of water with respect to the network; the sum of Eqs. **11** and **12** yields Eq. **3**. Eqs. **1**–**3** with boundary conditions and a constitutive equation for $\pi = \pi(\phi)$ (see *SI Text*) constitute our model. Because the height of the biofilm is always about 10–100 times smaller than the radius, we can reduce the model equations to the single PDE **5** for the height $h(r,t)$ (see *SI Text*).

†In ref. 30 the opposite assumption is made, which substantially differentiates the two models.

Asymptotic Analysis. For simplicity, we illustrate the model in two planar dimensions (x,z); the generalization to cylindrical symmetry is straightforward. A self-consistent thin film approximation and dominant balance of Eqs. **1**–**4** are outlined in the *SI Text* and yield:

$$h_t - K[Rh^3(gh)_x]_x = gh \qquad [13]$$

where K is given by Eq. **6**; the height is rescaled with the initial height h_0; x, R are rescaled with the initial radius R_0; g^{-1} is rescaled with the average division time and we consider the first stages of growth where $g \approx 1$. We expect nutrient limited growth to modify radial expansion after about 12 h when height saturation occurs.

To study the solution of this equation we first substitute $h = e^t H$ and obtain:

$$H_t = K(H^3 H_x)_x e^{3t} R. \qquad [14]$$

Rescaling time implicitly with $\partial\tau/\partial t = Ke^{3t}R$ yields:

$$H_\tau = (H^3 H_x)_x. \qquad [15]$$

We search for a self-similar solution of the form $H = F(\eta)/R(\tau)$ with $\eta = x/R(\tau)$ and obtain:

$$-(F\eta)' R_\tau / R^2 = (F^3 F_\eta)'/R^6. \qquad [16]$$

The time component of the above equation $R_\tau/R^2 = 1/R^6$ can be solved to obtain R observing that $R_t = R_\tau \partial\tau/\partial t = Ke^{3t}/R^3$ giving

$$R = (1 + 4Ke^{3t}/3)^{1/4}. \qquad [17]$$

At small times $R \sim 1$, whereas as $t \to \infty$, the exponential takes over and $R \sim e^{3t/4}$. The spatial component of Eq. **16** $-(F\eta)' = (F^3 F_\eta)'$ can be integrated once to give $-F\eta = F^3 F_\eta + b$ where $b = 0$ because $F \to 0$ for $\eta \to 0$. This yields the separable equation $-F\eta = F^3 F_\eta$, whose solution is $F = [c - 3\eta^2/2]^{1/3}$, where c is set by the initial condition:

$$h(x,t) = \frac{e^t}{R}\left[c - \frac{3}{2}\left(\frac{x}{R}\right)^2\right]^{1/3}. \qquad [18]$$

Note that as $x^* \to \sqrt{2c/3}R$, $h \to 0$ and $h_x \to -\infty$. We regularize the solution by assuming that the profile asymptotes to h_∞. Imposing $h(x^*) = h_\infty$ yields $[c - 3/2(x^*/R)^2]^{1/3} = h_\infty R$, and the evolution of the regularized slope reads

$$h_x(x^*) = -\sqrt{\frac{2c}{3}}\frac{e^{3t}}{R^4 h_\infty^2}. \qquad [19]$$

If h_∞ grows exponentially (as it seems to be the case initially for the wild-type biofilm), the exponent at the numerator decreases from $3t$ to t. At small time scales, when $R \sim 1$, the slope at x^* grows exponentially $h_x(x^*) \sim e^t$. Later on, when $R \sim e^{3t/4}$, the slope reaches a maximum value and then decreases to zero as $h_x(x^*) \sim e^{-2t}$.

The experiments confirm that after initially steepening, the profiles reach a maximum slope, and then become less steep, approaching a nonzero slope at long times (see Fig. 3*D*). Both height saturation and the precise dynamics of cells near the leading edge of the biofilm may affect this behavior. In fact, if the solution matches to a steady rather than a growing layer h_∞, the slope steepens at a faster rate $h_x^* \sim e^{3t}$ and then transitions to a constant value, without decreasing to zero.

In 2D cylindrical coordinates, the same arguments hold upon substituting $\partial_x \to 1/r(r\partial_r)$ so that Eq. **13** transforms into Eq. **5** and repeating the arguments applied to obtain **17**–**19**, with the ansatz $H = F(r/R)/R^2$ to fulfill mass conservation, one obtains Eqs. **7** to **9**.

Numerical Simulations. In order to obtain the entire solution linking the two behaviors outlined above, we perform finite difference simulations of Eq. **13** with no flux boundary conditions both at the center of the biofilm and at the end of the asymptotic layer. We use MATLAB's implicit solver *ode15s* for the time integration, and we discretize space with a second order central finite difference algorithm. The initial condition is taken to be $h(x,0) = e^{-x^4} + h_\infty$ so that $R_0 \approx 1$ and $h_0 \approx 1$. We take $h_\infty = 0.1$. The scalings demonstrated in the paper occur independently of the precise form of the initial conditions.

We compute the biofilm slope and radius by smoothening the experimental profiles shown in Fig. 3 *A* and *B* with a moving average algorithm, and finding the maximum slope. We vary the smoothening window from 50 to 300 μm and obtain 10 different realizations of R and h_x^*; in Fig. 3 *D* and *E* we plot the average, the error bar is the standard deviation.

ACKNOWLEDGMENTS. We are grateful to M. Vergassola and J. M. Ghigó for useful discussions and to Steven Branda for the *hag eps* mutant. This research was supported by a Marie Curie IO Fellowship within the 7th European Community Framework Programme to A.S., by the BASF Advanced Research Initiative at Harvard University, and by the National Science Foundation through the Harvard Materials Research Science and Engineering Center (DMR-0820484) and the Division of Mathematical Sciences (DMS-0907985). R.K. and H.V. were also supported by National Institutes of Health Grant GM58213.

1. Stewart PS, Franklin MJ (2008) Physiological heterogeneity in biofilms. *Nat Rev Microbiol* 6:199–210.
2. López D, Vlamakis H, Kolter R (2010) Biofilms. *Cold Spring Harb Perspect Biol* 2: a000398.
3. Ghannoum M, O'Toole GA (2004) *Microbial Biofilms* (ASM Press, Washington).
4. Branda SS, Vik A, Friedman L, Kolter R (2005) Biofilms: The matrix revisited. *Trends Microbiol* 13:20–26.
5. Flemming HC, Wingender J (2010) The biofilm matrix. *Nat Rev Microbiol* 8:623–633.
6. Branda SS, Chu F, Kearns DB, Losick R, Kolter R (2006) A major protein component of the *Bacillus subtilis* biofilm matrix. *Mol Microbiol* 59:1229–1238.
7. Kearns DB, Chu F, Branda SS, Kolter R, Losick R (2005) A master regulator for biofilm formation by *Bacillus subtilis*. *Mol Microbiol* 55:739–749.
8. Blair KM, Turner L, Winkelman JT, Berg HC, Kearns DB (2008) A molecular clutch disables flagella in the *Bacillus subtilis* biofilm. *Science* 320:1636–1638.
9. Fujita M, Gónzalez-Pastor JE, Losick R (2005) High- and low-threshold genes in the Spo0A regulon of *Bacillus subtilis*. *J Bacteriol* 187:1357–1368.
10. Vlamakis H, Aguilar C, Losick R, Kolter R (2008) Control of cell fate by the formation of an architecturally complex bacterial community. *Genes Dev* 22:945–953.
11. Henrichsen J (1972) Bacterial surface translocation: A survey and a classification. *Bacteriol Rev* 36:478–503.
12. Aguilar C, Vlamakis H, Guzman A, Losick R, Kolter R (2010) KinD is a checkpoint protein linking spore formation to extracellular-matrix production in *Bacillus subtilis* biofilms. *MBio* 1:1–7.
13. Tanaka T, Fillmore DJ (1979) Kinetics of swelling of gels. *J Chem Phys* 70:1214–1218.
14. Landau LD, Lifshitz EM (1980) *Course of Theoretical Physics vol V—Statistical physics* (Elsevier, Oxford, UK).
15. De Gennes PG (1979) *Scaling Concepts in Polymer Physics* (Cornell Univ Press, Ithaca, NY).
16. Doi M, Onuki A (1992) Dynamic coupling between stress and composition in polymer solutions and blends. *J Phys II* 2:1631–1656.
17. Oron A, Davis SH, Bankoff SG (1997) Long-scale evolution of thin liquid films. *Rev Mod Phys* 69:931–980.
18. Klapper I, Rupp C, Cargo R, Purvedori R, Stoodley P (2002) Viscoelastic fluid description of bacterial biofilm material properties. *Biotechnol Bioeng* 80:289–296.
19. Shaw T, Winston M, Rupp CJ, Klapper I, Stoodley P (2004) Commonality of elastic relaxation times in biofilms. *Phys Rev Lett* 93:098102.
20. Wilking JN, Angelini TE, Seminara A, Brenner MP, Weitz DA (2011) Biofilms as complex fluids. *MRS Bull* 36:385–391.
21. Deboeuf AD, Gauthier G, Martin J, Yurkovetsky Y, Morris JF (2009) Particle pressure in sheared suspension: A bridge from osmosis to granular dilatancy. *Phys Rev Lett* 102:108301.
22. Martinez A, Torello S, Kolter R (1999) Sliding motility in mycobacteria. *J Bacteriol* 181:7331–7338.
23. Fall R, Kearns DB, Nguyen T (2006) A defined medium to investigate sliding motility in a *Bacillus subtilis* flagella-less mutant. *BMC Microbiol* 6:31–42.
24. Kinsinger RF, Shirk MC, Fall R (2003) Rapid surface motility in *Bacillus subtilis* is dependent on extracellular surfactin and potassium ion. *J Bacteriol* 185:5627–5631.
25. Kearns DB (2010) A field guide to bacterial swarming motility. *Nat Rev Microbiol* 8:634–644.
26. Short MB, et al. (2006) Flows driven by flagella of multicellular organisms enhance long-range molecular transport. *Proc Natl Acad Sci USA* 103:8315–8319.
27. Romero D, Aguilar C, Losick R, Kolter R (2010) Amyloid fibers provide structural integrity to *Bacillus subtilis* biofilms. *Proc Natl Acad Sci USA* 107:2230–2234.
28. Chu F, Kearns DB, Branda SS, Kolter R, Losick R (2006) Targets of the master regulator of biofilm formation in *Bacillus subtilis*. *Mol Microbiol* 59:1216–1228.
29. Branda SS, González-Pastor JE, Ben-Yehuda S, Losick R, Kolter R (2001) Fruiting body formation by *Bacillus subtilis*. *Proc Natl Acad Sci USA* 98:11621–11626.
30. Cogan NG, Keener JP (2004) The role of the biofilm matrix in structural development. *Math Med Biol* 21:147–166.
31. Tanaka H (1997) Viscoelastic model of phase separation. *Phys Rev E* 56:4451–4462.